Two-deuteron radiative capture: Polarization observables at $E_d \leq 15$ MeV

J. L. Langenbrunner and H. R. Weller
Duke University and Triangle Universities Nuclear Laboratory, Duke Station, Durham, North Carolina 27706

D. R. Tilley
North Carolina State University, Raleigh, North Carolina 27695
and Triangle Universities Nuclear Laboratory, Duke Station, Durham, North Carolina 27706

(Received 3 November 1989)

Measurements of the ^{2}H($\vec{d},\gamma$)^{4}He cross section $\sigma(\theta)$, the vector analyzing power $A_y(\theta)$, and the tensor analyzing power $A_{yy}(\theta)$ have been obtained at E_d(lab)=14.7 and 1.2 MeV and E_d(lab)$\leq$0.8 MeV; the spherical tensor analyzing power $T_{20}(\theta)$ was also measured at E_d(lab)=14.7 MeV. $A_y(130°)$ and $A_{yy}(130°)$ were measured at eight bombarding energies between E_d(lab)=0.8 and 14.7 MeV and $T_{20}(130°)$ at ten energies between E_d(lab)=5.4 and 14.7 MeV. A transition-matrix element analysis is performed by fitting to the available angular distribution data at E_d(lab)$\leq$0.8 MeV and at E_d(lab)=1.2 and 14.7 MeV. The data are compared to the results of a multichannel resonating group model (MCRGM) calculation. The MCRGM model includes the tensor force in calculating both the continuum and bound states and provides a fairly good description of the data, especially above E_d=5 MeV. This calculation predicts a D-state probability in ^{4}He arising from the relative motion between the two deuterons of P_D=2.2%.

I. INTRODUCTION

The first experimental evidence which indicates that the ^{2}H(d,γ)^{4}He reaction is sensitive to the ^{4}He D state was obtained from measurements of the tensor analyzing power $T_{20}(\theta)$ at E_d(lab)=9.7 MeV.[1] At this energy the reaction proceeds predominantly via $E2$ radiation and the tensor analyzing power is the result of interference of the dominant d-wave capture amplitude leading to the S state of ^{4}He with s- and d-wave capture amplitudes leading to the D state of ^{4}He.

The model used to interpret the data in Ref. 1 was a direct capture model which assumed point deuterons. This model has been exploited and refined by a number of authors.[2–4] The effects of the deuteron D state,[5] the inclusion of other (non-$E2$) multipoles,[3] and sensitivities to various forms of the bound and continuum wave functions[2,4] have been examined over a broad range of energies from 50 keV to 50 MeV. Reference 6 provides a rather recent review of most of these calculations and the relevant experimental results.

Inasmuch as the ^{2}H(d,γ)^{4}He reaction can be viewed as a one-step process between initial and final states having total isospin T=0, the probability amplitudes for the transition can be calculated using the isoscalar components of the electromagnetic operators. $E1$ radiation is forbidden to first order in this reaction for two reasons. First, since $l+S$ must be even in the incident channel formation, a 1^- state requires S=1. The ground state of ^{4}He is primarily L=0, S=0, therefore the $E1$ transition would be ΔS=1. Second, the incident channel has T=0, hence this is a ΔT=0, $E1$ transition which is forbidden since it violates the isospin selection rule that $\Delta T=\pm 1$ for $E1$ transitions in self-conjugate nuclei.[7] Furthermore, the fact that the particles in the entrance channel are identical can be shown to prohibit $E1$ radiation resulting from charge polarization of the deuterons.[8] The isospin selection rules in Ref. 7 also imply that ΔT=0, $M1$ transitions in self-conjugate nuclei are inhibited by about a factor of 100; this transition must in any case lead to the small D state of ^{4}He. We therefore expect the reaction to be dominated by $E2$ radiation. Direct capture calculations based on these ideas have been fairly successful in describing the data of this reaction, especially for a deuteron bombarding energy of $\sim$10 MeV.[3]

A more fundamental calculation, based on the multichannel resonating group model (MCRGM), is now available.[9] This calculation uses an effective two-nucleon force as a starting point. The two-body tensor force gives rise to a D state in the calculated ^{4}He ground-state wave function. This tensor force is present in both the bound and the continuum parts of the calculation (unlike the direct capture model calculations), and is therefore more consistent than the direct capture model calculations. Furthermore, coupling between the $d+d$, the $p+^3$H, and the $n+^3$He channels produces, upon proper antisymmetrization, $E1$ radiation. These apparently important couplings are not present in the direct capture model, which only gives $E1$ radiation as a result of the spin-dependent part of the $E1$ operator.[3,10,11]

The first clear experimental evidence for non-$E2$ radiation in the ^{2}H(d,γ)^{4}He reaction was a measurement of the vector analyzing powers at E_d=10 MeV.[12] This data set was shown to indicate that both $E1$ and $M2$ radiation was present, each at about the 3% level. A later measurement[10] at 1.2 MeV was shown to be consistent with results of the MCRGM calculation, which indicates that the radiation consisted of almost equal admixtures of $E2$, $E1$, and $M2$ radiation at this energy.

This major change in the nature of radiation between

10 and 1 MeV is the subject of study of the present work. Since the extrapolation of the cross section to 10–20 keV is necessary to determine the astrophysical S factor,[4,6] it seems desirable to understand how the reaction changes its nature as the energy drops from 10–15 MeV down to these very low energies. Furthermore, if we can understand the nature of the reaction in more detail, we may be able to choose experimental conditions that make a determination of the D state in ^{4}He most straightforward. Previous efforts, which based extrapolations to low energies on a direct capture–pure $E2$ model and attributed all s-wave capture to the D state of ^{4}He, must be reexamined in light of these new data and calculations.[4,9]

The goal of the present experimental work is to provide angular distributions and excitation functions of the cross section, tensor, and vector analyzing powers with polarized deuteron beams ranging in energy from below 0.8 MeV up to 15 MeV. Data over this energy region will be presented and compared to the results of the MCRGM model calculation in an attempt to see how the physics of the reaction changes with energy, what the role of non-$E2$ radiation is, and how the D state of ^{4}He influences the data. It will be seen that the MCRGM calculation gives a good description of much of the data. A model-independent transition-matrix element analysis was also performed and provides detailed information regarding the various T-matrix elements that contribute to the reaction. These results are also compared to the results of the MCRGM calculations.

II. EXPERIMENT

The present data on the $^2\mathrm{H}(\vec{d},\gamma)^4\mathrm{He}$ reaction obtained at Triangle Universities Nuclear Laboratory (TUNL) include $\sigma(\theta)$, $A_y(\theta)$, and $A_{yy}(\theta)$ for $\langle E_d(\mathrm{lab})\rangle = 14.7$ and 1.2 MeV and $\langle E_d(\mathrm{lab})\rangle \leq 0.8$ MeV as well as $T_{20}(\theta)$ data at $\langle E_d(\mathrm{lab})\rangle = 14.7$ MeV. $A_y(130°)$, $A_{yy}(130°)$, and $T_{20}(130°)$ were measured as a function of laboratory energy between 0.8 and 15 MeV. The TUNL FN-tandem Van de Graaff provided deuteron beams with energies as low as $E_d = 2.29$ MeV and as high as $E_d = 15.0$ MeV. Lower-energy polarized deuteron beams could not be produced directly with the FN-tandem accelerator due to poor beam transmission (less than 20%) at very low terminal potentials. The beam was therefore degraded in energy by placing one-to-four Havar foils at the entrance to the target. Each Havar degrading foil has a nominal areal density of 5.27 mg/cm^2 (thickness of 6.4×10^{-4} cm). The target conditions used for various energies are given in Table I.

A solid-state detector, calibrated at 5.48 MeV by means of an ^{241}Am source, was used in two configurations in order to measure the beam energy and beam energy spread. First, to deduce the energy and energy spread due to the foils alone, the beam that had traversed the Havar foil was scattered from a thin ($\sim$5 μg/cm^2) ^{12}C foil from which the elastically scattered deuterons were detected in a scattering chamber at 40°. Second, to deduce the effect on the beam's energy as a result of passing through the foils plus gas, elastically scattered deuterons of known energy were detected by a solid-state detector contained in a small chamber having a Havar foil entrance window and containing deuterium gas whose pressure could be varied. It was found, for example, that a deuteron beam of $E_d = 3.4$ MeV incident on four consecutive 6.4×10^{-4} cm Havar foils produced a beam of 0.80 MeV$\pm$3% with full width at half maximum of 130 keV. Our measurements for energy loss in Havar and D_2 gas agree (5%) with previous experimental results for the energy loss of deuterons through Havar,[13] and are also in agreement with the results of calculations based on the equations of Bethe and Ashkin[13] (3%).

The cylindrical gas cell used for the low-energy measurements (at and below $\langle E_d\rangle = 1.2$ MeV) was 1.27 cm long and was oriented such that it was axially symmetric with respect to the beam axis, as in Fig. 1. This cell was electrically insulated from the beam pipe. An electron suppressor ring (operated at -300 V) immediately preceded the cell in order to prevent electrons from escaping from the cell. The gas cell was operated at room temperature (air cooled) at a pressure of 827 kPa, sufficient to stop the beam in the case of $\langle E_d\rangle \leq 0.8$ MeV. The deuterons which are stopped in the gas should be viewed as having energies extending from their entrance value down to zero.

TABLE I. Energy conditions and observables for various target configurations. Energy values are given in the laboratory reference frame. $\langle E_d(\mathrm{lab})\rangle$ is the center-of-target energy.

E_{beam} (MeV)	No. of 6.4×10^{-4} cm Havar foils	Gas pressure (kPa)	E_{max} (MeV)	E_{min} (MeV)	$\langle E_d\rangle$ (MeV)	Observable
3.4	4	827	0.8	0	$\leq$0.8	A_{yy}, A_y
3.3	3	896	1.6	0.6	1.2	A_{yy}, A_y
2.29	2	827	0.8	0	$\leq$0.8	σ
2.28	1	896	1.6	0.6	1.2	σ
2.5	2	145	1.1	0.7	0.9	σ
2.5	1	193	1.9	1.6	1.8	σ
3.0	1	193	2.4	2.2	2.3	σ
3.85	1	290	3.4	3.1	3.3	σ
5.0	1	290	4.6	4.4	4.5	σ
10.0	Ta foil	414 cooled	9.7	9.4	9.6	$T_{20}, A_{yy}, A_y, \sigma$
15.0	Ta foil	414 cooled	14.8	14.6	14.7	$T_{20}, A_{yy}, A_y, \sigma$

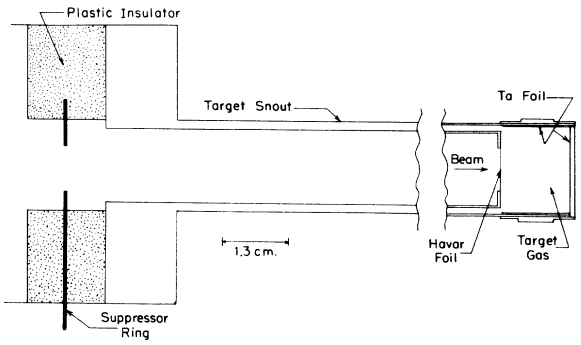

FIG. 1. The stainless-steel target snout and Faraday cup for low-energy beams are shown (to scale). The entire assembly is isolated from the beam pipe by a plastic insulator. A negative voltage is placed on the suppressor ring to reflect low-energy electrons from the tantalum collimator, which precedes this assembly and Havar entrance foil. The 1.27 cm gas cell is lined with thin tantalum foil (0.25 cm) and is operated at an absolute D_2 gas pressure of 827 kPa. The wall thickness of this cell was varied using a machined sleeve in order to attenuate γ rays equally for the various angle positions of the γ-ray detectors.

The target for the 15 MeV beam consisted of a liquid-nitrogen–cooled cylindrical gas cell, 1.9 cm in diameter, operated at 414 kPa (target thickness of 4.92 mg/cm^2). For this target, the symmetry axis was perpendicular to the reaction plane. Tantalum entrance and exit windows were 6.4×10^{-4} cm thick (10.54 mg/cm^2) and a suppressed Faraday cup was positioned 7 cm in back of the target to integrate the beam. The bombarding beam of 15.0 MeV was calculated to be degraded in energy to 14.76 MeV by the entrance foil; the gas degrades the beam energy to 14.6 MeV. The center-of-target energy was $\langle E_d \rangle = 14.7$ MeV. This target was also utilized in obtaining the data for $A_{yy}(130°)$, $A_y(130°)$, and $T_{20}(130°)$ as a function of energy between $E_d = 5.4$ and 15 MeV.

Polarized deuteron beams were produced using the TUNL Lamb-shift source equipped with a spin filter[14] and a Wien filter. Beam intensities of 30–70 nA were available on target. The percentage of beam polarization (P) was measured via the quench ratio method[15] after intervals of about 1 h. Our values for P were checked by measuring analyzing powers for $^{12}C(\vec{d},d)$ at $E_d = 7$ MeV and comparing with previous results for A_y (Ref. 16) and A_{yy} (Ref. 17). The results for the percentage beam polarization (P) deduced from each of these methods agreed within the quoted error of 5% of unity (P is typically 0.66 ± 0.03).

The capture γ rays in the $^2H(d,\gamma)^4He$ reaction are relatively energetic (Q value = 23.8 MeV). In order to reduce the background, each of the NaI(Tl) detectors is contained in a well-type NE110 plastic scintillator shield which is operated in the anticoincidence mode. The detector assemblies were also surrounded by passive shielding: 10 cm of lead, 20 cm of paraffin doped with lithium carbonate and a 1.5 cm thick sheet of plastic containing boron (or 0.15 cm of sheet-metal cadmium). This reduces the neutron background from the $^2H(d,n)^3He$ reaction and other neutrons produced by the beam hitting collimators, foils, or the beam stop. Essentially all of the background events present in the spectra of our two anticoincidence-shielded 25×25 cm NaI(Tl) spectrometers[18] in the region of interest were due to unrejected cosmic-ray background. This was subtracted out in the final results by summing the cosmic events at higher energies and extrapolating them into the region of the data. Both detectors' responses to the cosmic rays were measured in a separate run and found to be flat as a function of energy in this energy region.

The data for $\sigma(\theta)$ at $\langle E_d \rangle \leq 0.8$ and $\langle E_d \rangle = 1.2$ MeV were taken by using one of our NaI(Tl) spectrometers as a monitor (placed at $\theta_{lab} = 130°$) and rotating the other through forward angles. The ratio of yields should give a reliable measurement of the angular dependence of $\sigma(\theta)$. Spectra from each detector were analyzed by fitting the γ_0 transition with the previously determined NaI detector response function obtained using the $^3H(p,\gamma)^4He$ reaction. At low energies, the beam energy spread contributes to the width of the γ-ray response function. Measured yields were obtained by summing over a γ-ray energy region corresponding to one line-shape width below the peak centroid energy and up to one width above it. The absolute value of the differential cross section $\sigma(\theta)$ was then obtained by comparing the product of detector efficiency times yield obtained with the spectrometer at forward angle θ with that of the stationary NaI monitor detector. The efficiency of the NaI spectrometers has been previously determined.[18] The target thickness is expected to be accurate to 1%.

The cross section obtained at our lowest energy (≤ 0.8 MeV) contains the following systematic errors: determining absolute efficiency and determining line shape (~20%) and determining target thickness and beam integration (~20%). To check for beam ion implantation in the Havar entrance foils, the gas cell was filled with ^{4}He gas in place of deuterium gas and spectra were taken. Capture reactions for ^4He+d are energetically small compared to the $d+d$ reaction; this procedure is expected to show γ rays resulting from beam implantation in the Havar foils. The effect of beam implantation on the γ-ray yield leads to a correction of about 3% at each measured angle for $\langle E_d \rangle \leq 0.8$ MeV, small compared to statistical error. Corrections were also made for effects due to dead time and accidental coincidences; these were approximately 1% at low energy and about 10% at 14.7 MeV. Typical anticoincidence spectra at $\langle E_d \rangle = 14.7$ MeV and $\langle E_d \rangle \leq 0.8$ MeV are shown before background subtraction in Fig. 2.

Vector and tensor analyzing powers (A_y, A_{yy}, T_{20}) involve the ratios of yields and thereby avoid systematic errors associated with determining the absolute values of detector efficiency and target thickness. In the Madison convention (Ref. 19), the A_y and A_{yy} measurements correspond to setting $\beta = 90°$ and $\phi = 0°$, where β designates the angle between the deuteron-spin axis and the beam-momentum axis and ϕ is the angle between the spin axis and the normal to the reaction plane ($\mathbf{k}_{in}\times\mathbf{k}_{out}$). We have the equations

$$A_y(\theta)=\frac{1}{P}\frac{Y_1(\theta)-Y_3(\theta)}{Y_1(\theta)+Y_2(\theta)+Y_3(\theta)}\ , \tag{1}$$

$$A_{yy}(\theta)=\frac{1}{P}\frac{Y_1(\theta)+Y_3(\theta)-2Y_2(\theta)}{Y_1(\theta)+Y_2(\theta)+Y_3(\theta)}\ , \tag{2}$$

where Y_1, Y_2, Y_3 are the normalized yields at angle θ corresponding to the deuterons in substate populations $m=1,0,-1$, respectively, and P is the percentage of the beam with the desired polarization moment.[15] The spherical tensor analyzing power T_{20} measurements were obtained by setting $\beta=0°$ and $\phi=90°$. The expression for $T_{20}(\theta)$ is then given by

$$T_{20}(\theta)=\frac{\sqrt{2}}{P}\frac{Y_1(\theta)-Y_2(\theta)}{2Y_1(\theta)+Y_2(\theta)}\ , \tag{3}$$

where $Y_1(\theta)$ is the yield for $m=1$ and $Y_2(\theta)$ is the yield for $m=0$ deuterons. Equal amounts of data were taken with the spin-symmetry axis both parallel and antiparallel to the beam momentum in order to reduce the possible effect of count-rate asymmetries due to small, spurious beam polarization moments. The Cartesian tensor analyzing power $A_{yy}(\theta)$ is related to the spherical tensor analyzing powers via the expression

$$A_{yy}(\theta)=-T_{20}(\theta)/\sqrt{2}-\sqrt{3}T_{22}(\theta)\ . \tag{4}$$

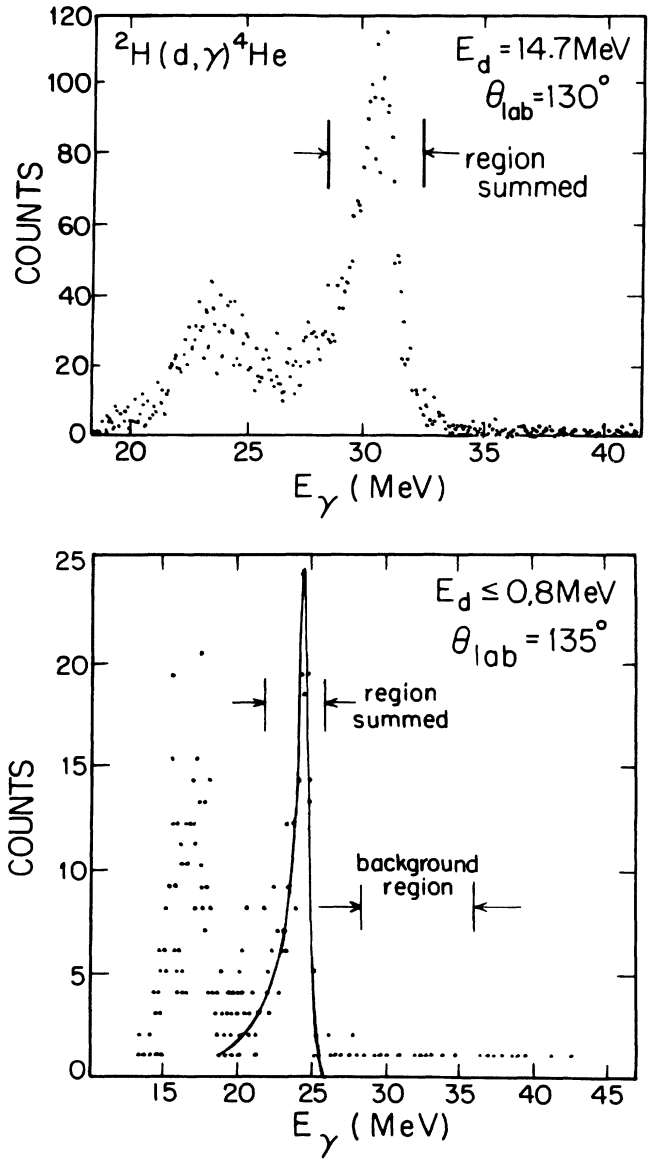

FIG. 2. Spectra at $\langle E_d\rangle=14.7$ MeV and $\langle E_d\rangle\leq 0.8$ MeV with summing regions indicated. The solid line in the low-energy spectrum is a smooth curve drawn through the data points.

Concern for depolarization effects at low energies is based on a comparison of the period of the atomic Larmor precession for the deuteron (~ 3 ns) with the time a deuteron typically spends traversing the target (~ 1 ns) (e.g., Ref. 20). To test for depolarization, a gas cell was fitted with a tritiated titanium target positioned at the back end of the cell. Deuterium gas filled the region between the entrance window and the tritiated target. As the D_2 gas pressure was raised in the gas cell, the deuterium beam energy incident on the tritium target fell below 100 keV where the ^{3}H$(d,n)^4$He reaction is known to proceed almost totally through s-wave deuterons.[21] The beam was stopped in the titanium foil. The known analyzing powers from the ^{3}H$(\vec{d},n)^4$He reaction[21] were used to deduce the beam polarization (P) at the lowest energies, after the beam had traversed the entrance foils and the D_2 gas. The neutron flux was measured by means of a commercially available (5 cm×5 cm) NE213 scintillator placed at 0° with respect to the beam. A pulsed (4 MHz) deuteron beam allowed us to use the time-of-flight technique to identify the proper outgoing neutrons. Neutrons from the ^{3}H(d,n) reaction were separated by 20 ns over a flight path of about 1 m. The result was $P=0.68\pm0.03$ for an incident beam with bombarding energy of 3.375 MeV degraded to 0.80 MeV by Havar and subsequently traveling through the D_2 gas, entering the tritium target with energy less than 100 keV. This was the same value of P as that deduced using the quench ratio method. No depolarization was observed as the beam energy was decreased (achieved by increasing the D_2 gas pressure). In addition, this method was used to estimate the effective target thickness of the gas at $\langle E_d\rangle\leq 0.8$ MeV by measuring the range of the beam in the D_2 gas. Neutrons from the ^{3}H(d,n) reaction were not produced when the deuterium gas pressure was greater than 207 kPa absolute in the 1.9 cm gas gell (i.e., 0.69 mg/cm^2).

III. MODEL RESULTS AND COMPARISON TO DATA

Weller *et al.*[1] were able to account for $\sigma(\theta)/A_0$ and $T_{20}(\theta)$ observed in the ^{2}H$(\vec{d},\gamma)^4$He reaction at E_d(lab)=9.7 MeV with a direct capture model that included a small admixture of $L=2$ strength in the ground state of ^{4}He. It is important to note that within that model, the observable $T_{20}(\theta)$ would be zero if there were

no D state in ^{4}He. The model used the simplifying assumption of pure $E2$ radiation. This assumption was also made in subsequent studies to describe the cross section data below $E_d=1$ MeV, but no analyzing powers were used to test for other multipoles at low energies. We find that when we compare the present MCRGM model results to all observables over the energy range of the present experiment, the assumption of pure $E2$ radiation is a fair approximation (at the 10% level) above 10 MeV, but is not necessarily valid below about $E_d=5$ MeV.

The multichannel resonating group model (MCRGM) calculation presented here is described in detail in Ref. 9. This calculation includes s, p, and d waves in the incident channel and considers $E1$, $M1$, $E2$, and $M2$ transitions. The full form of the operators in the long-wavelength approximation, including spin-dependent terms, was used. The calculation treats the ground state and continuum states in a consistent manner. The p-T and n-^{3}He channels are included along with the d-d channel. All fragments (d,^{3}H,^{3}He) are included in this calculation, but without D state components. Although the $^5s_2$ state can decay to the $^5D_0$ component of the ^{4}He ground state, there is no contribution from the intrinsic deuteron D state. The effective two-body force used in this calculation predicted a D-state probability of 2.2% in the ^{4}He ground state.[9,10] Note that this does not represent the entire D-state probability in ^{4}He, but only the part associated with the $L=2$ relative motion of the two (S-state only) deuterons.

The energy-dependent cross-section data and model calculations are presented here in terms of the astrophysical factor $S(E)$ defined by

$$S(E_{\text{c.m.}})=\sigma(E_{\text{c.m.}})E_{\text{c.m.}}\exp(2\pi\eta) \quad (5)$$

with $2\pi\eta=31.40(E_{\text{c.m.}})^{-1/2}$ for the ^{2}H$(d,\gamma)^4$He reaction. $E_{\text{c.m.}}$ is the center-of-mass energy in keV and $\sigma(E_{\text{c.m.}})$ is the angle integrated cross section in barns. The data and the results of the MCRGM model calculation are presented in Fig. 3. The MCRGM model (dashed line) gives a very good description of the magnitude of the absolute cross section above $E_{\text{c.m.}}=400$ keV, including $E_{\text{c.m.}}=7.35$ MeV. Note that the absolute magnitudes of the calculated cross section have not been nor-

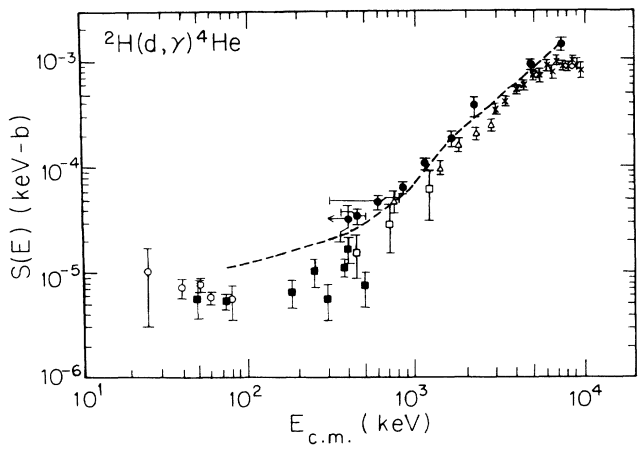

FIG. 3. The astrophysical factor $S(E)$ as a function of energy for the ^{2}H$(d,\gamma)^4$He reaction with present and previous data: Ref. 30, closed squares; Ref. 31, open circles; Ref. 32, open squares; Ref. 24, triangles; Ref. 23, crosses; present data, closed circles. The dashed line is the result of the MCRGM model calculation. The error bars represent the statistical uncertainties associated with the data points.

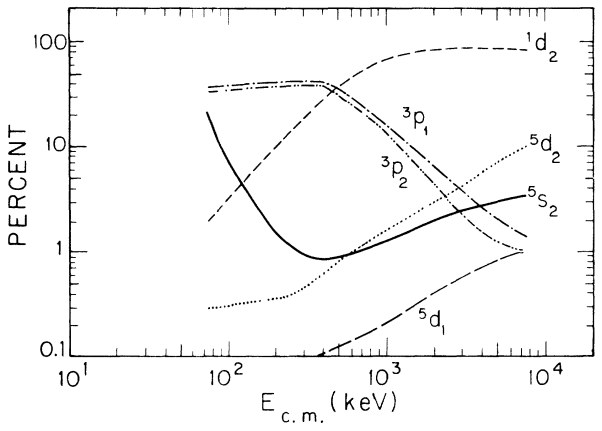

FIG. 4. Contributions to the total cross section by percentage are indicated by the quantum numbers of the incoming $d+d$ partial wave for the MCRGM model.

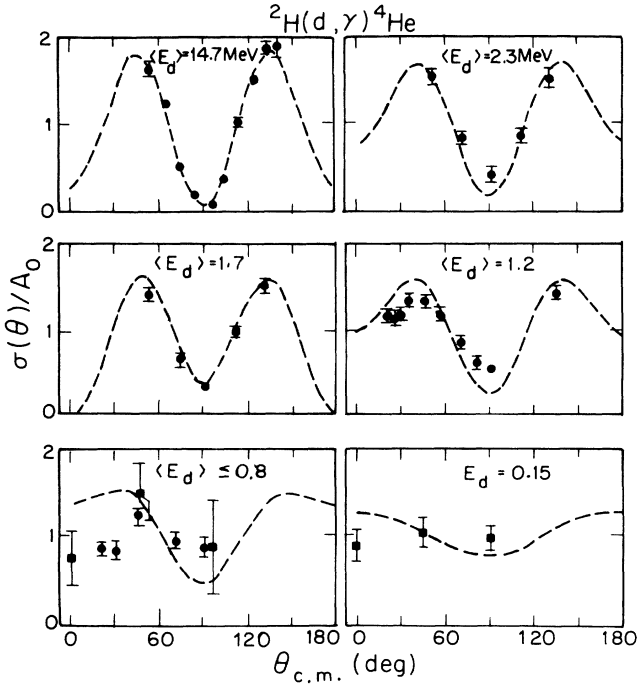

FIG. 5. Angular distributions in the center-of-mass frame for the cross section for the ^{2}H$(d,\gamma)^4$He reaction at laboratory energies $\langle E_d(\text{lab})\rangle$. The solid circles are the present data and the open circles are data of Ref. 30. The dashed curves represent the results of the MCRGM model calculations. The model calculations are energy averaged to represent the beam energy loss in the gas cell. The error bars represent the statistical uncertainties associated with the data points.

malized to the data.

The results of the MCRGM model for the percentage contribution of each transition amplitude to the total cross section as a function of deuteron energy in the center-of-mass system are shown in Fig. 4. Because of the centrifugal barrier, the contribution from the $^1d_2$ wave decreases rapidly with decreasing energy. The contribution of the $^1d_2$ wave is only of the order of a few percent at $E_{\text{c.m.}}=75$ keV. There are substantial contributions from the $^3p_1$ and $^3p_2$ terms (both at $\sim 40\%$) below $E_{\text{c.m.}}=400$ keV, the effects of which are most clearly seen in the polarization observables $A_y(\theta)$ and $A_{yy}(\theta)$. The $M1$ transition $^5d_1$ is small everywhere, rising to 1% near $E_{\text{c.m.}}=7$ MeV.

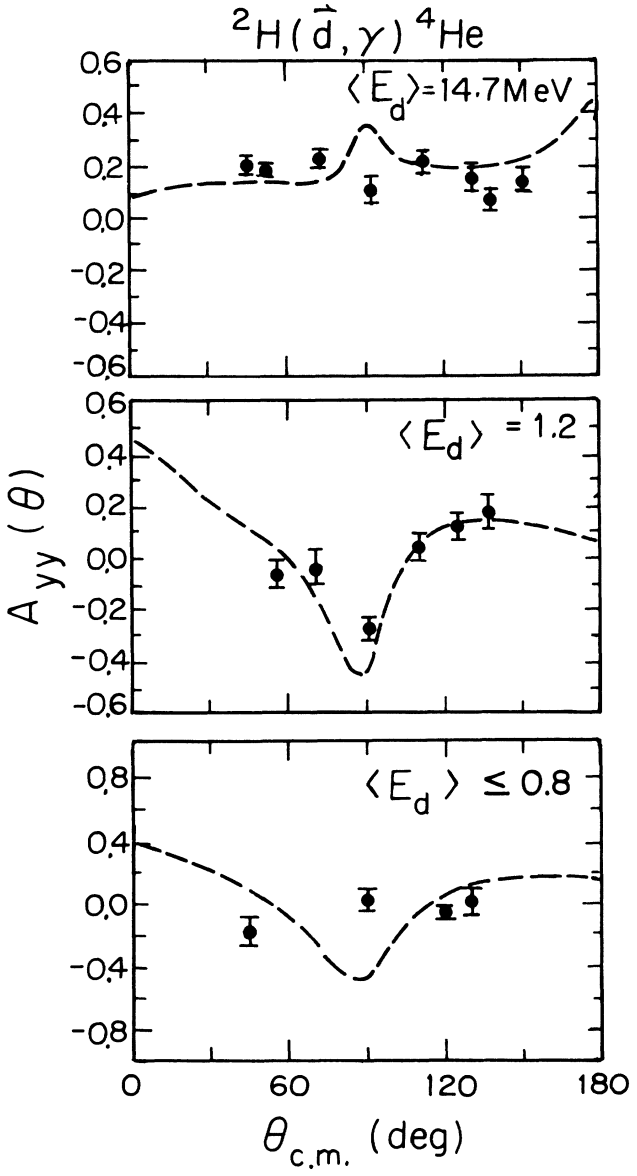

FIG. 6. Angular distribution of $A_{yy}(\theta)$ at $\langle E_d(\text{lab})\rangle$ shown with statistical uncertainties. The calculations are energy averaged in order to represent experimental conditions. The dashed curves represent the MCRGM model results. Pure $E2$ $^5s_2$-wave capture would result in an isotropic value for $A_{yy}(\theta)$ of 0.25.

In Fig. 5, the shape of the cross section $\sigma(\theta)/A_0$, where $4\pi A_0$ equals the angle integrated cross section, is shown over the energy range from $\langle E_d\rangle=14.7$ MeV to $\langle E_d\rangle=0.15$ MeV along with the MCRGM model results. As the energy decreases, the cross section changes from the characteristic $\sin^2 2\theta$ shape indicating d-wave capture $^5d_2(E2)\rightarrow{}^1S_0$, to a shape that includes appreciable strength at 90°. The cross section must be isotropic for 100% s-wave capture. Previous work[1,4,5,22–24] attributed all the strength at 90° from $E_{\text{c.m.}}=50$ keV to $E_{\text{c.m.}}=10$ MeV to s-wave $E2$ capture, an assumption which is not borne out by the polarization data. The MCRGM model predicts only 27% s-wave capture at $E_{\text{c.m.}}=75$ keV and nearly equal amounts of both $E1$ and $M2$ of nearly 35% each.

It should be noted that the model calculations have been energy averaged to represent the experimental con-

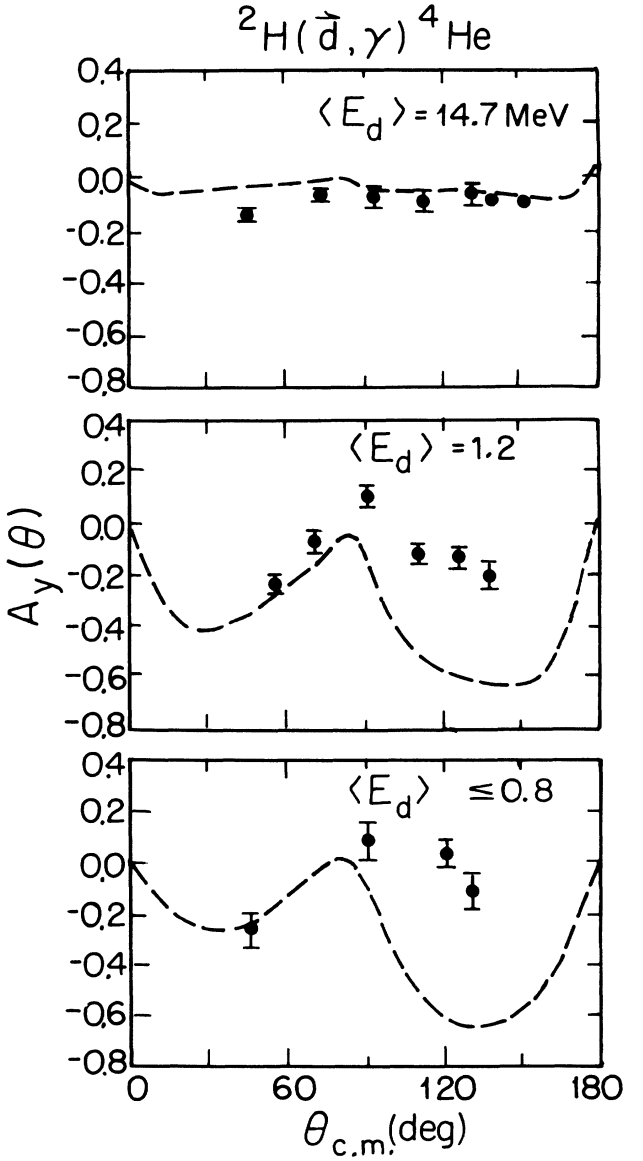

FIG. 7. Angular distributions of $A_y(\theta)$ shown with statistical uncertainties and with calculations as in Fig. 6.

ditions. For example, observables were calculated for three energies around $\langle E_d \rangle = 1.2$ MeV and for six energies below 0.8 MeV. The calculated observables were then weighted by the calculated cross section and averaged over the appropriate energy region to give the model results as plotted in Figs. 5–8. The MCRGM model describes the 1.2 MeV $A_{yy}(\theta)$ data well and indicates that this observable results mainly from the $S=1$, $E1$ and $M2$ amplitudes interfering with themselves.[10]

Corrections have been made to the cross-section data

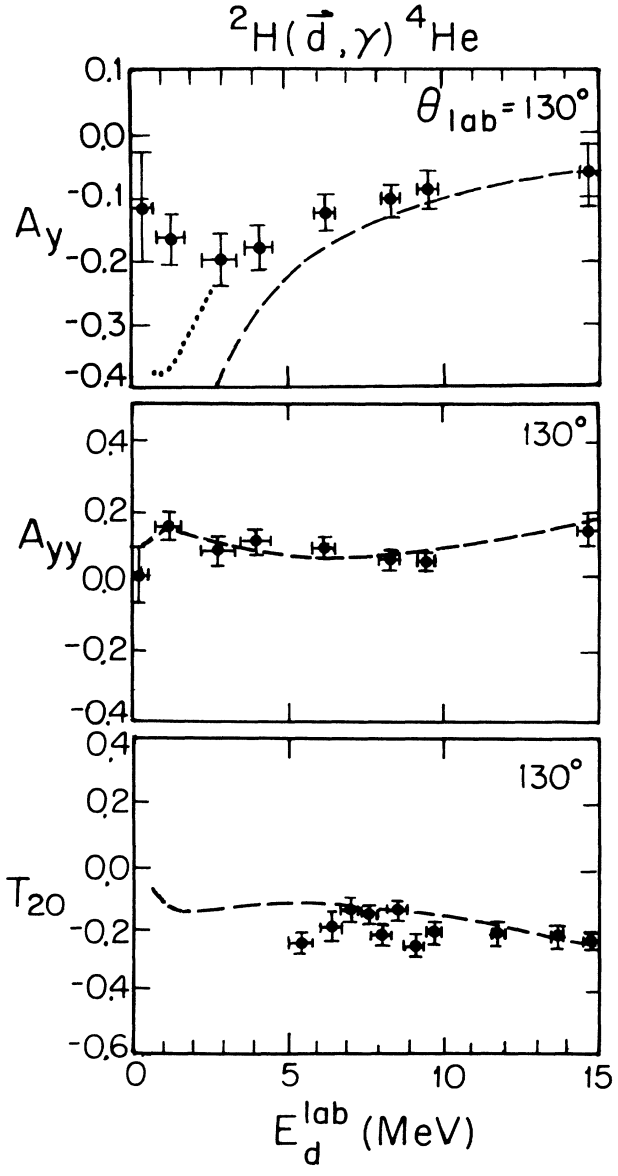

FIG. 8. The data for A_y, A_{yy}, and T_{20} at $\theta_{lab}=130°$ as a function of $\langle E_d(\text{lab}) \rangle$. The data are shown with horizontal bars to represent the energy thickness of the target and vertical bars to show the statistical uncertainties. The calculations are energy averaged to represent the experimental conditions. The dotted curve in the A_y (130°) case is the MCRGM calculation multiplied by 0.6. See also Ref. 36 for a discussion of the A_{yy} and A_y data as a function of deuteron bombarding energy up to 50 MeV.

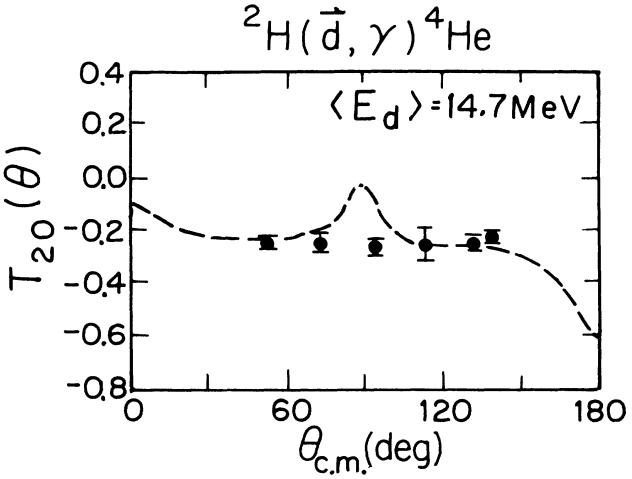

FIG. 9. Data for $T_{20}(\theta)$ at $\langle E_d \rangle = 14.7$ MeV with MCRGM calculations and statistical errors as in previous figures.

to account for the finite geometry of the detectors.[25] Figure 5 shows the point geometry angular distributions of the cross section. In most cases, the corrections due to finite geometry of the detectors are small (less than 2%) except at angles near 90° (e.g., a reduction of the cross section by 6% at $\theta=90°$ at 2.3 MeV and by 24% at $\theta=90°$ at 14.7 MeV). The data for the polarization observables in Figs. 6–9 have not been corrected for the finite geometry of the detectors, but these effects were found to be small compared to the statistical error. The effects were determined by comparing the model calculations of the angular distributions of $A_{yy}(\theta)$ and $A_y(\theta)$ assuming point geometry to the angular distributions which would have been observed using the experimental geometry. In the worst case, for $A_{yy}(90°)$ at $E_d=1.2$ and 14.7 MeV, the corrections amount to less than 20% of the statistical uncertainty.

Figure 7 shows the vector analyzing power $A_y(\theta)$, which arises from products of transition-matrix elements satisfying the triangle relation $\mathbf{S}+\mathbf{S}'=1$. The MCRGM model predicts very large values for $A_y(\theta)$ and predicts it to be very asymmetric about 90°. The deviation from the data reflects the fact that, as stated in Ref. 9, the calculated $d+d$ threshold in the MCRGM calculation is too low in energy so that the nearby 1^- ($E1$) and 2^- ($M2$) resonances contribute more than in reality. It is not clear from the vector polarization data which of either $E1$ or $M2$ radiation contributes at energies below $E_d=3$ MeV. In the MCRGM model *both* $^3p_1$ ($E1$) and $^3p_2$ ($M2$) contribute at essentially equal levels; this produces the large values for A_y at back angles through an $E1/M2$ interference term which is asymmetric about 90°.

The $A_y(E)$ data at $\theta=130°$ are shown as a function of energy in Fig. 8 along with the model results. The $A_y(E)$ data are sensitive to the p-wave strength and peak near $E_d=3$ MeV with a value of -0.2. The dramatic effect in $A_y(E)$ can be clearly seen at the lower energies. The MCRGM model overestimates $A_y(E)$ by a factor of 2 at $E_d=3$ MeV and this discrepancy grows with decreasing energy.

TABLE II. Results of fitting the available data simultaneously with selected multipoles, $\langle E_d \rangle = 14.7$ MeV.

Allowed multipole	χ^2	χ^2/ν	Partial contribution to the total cross section (%) by γ multipolarity $M1$	$E1$	$M2$	$E2$
$E2$	141.2	5.4				100
$E2,M1,E1$	43.8	1.9	0.6±1.3	3.5±1.2		95.9±2.2
$E2,M1,M2$	43.7	1.9	0.2±2.6		2.7±1.9	97.1±3.0
No ^{4}He D state[a]	157.1	6.5		15.5±2.0	7.8±3.7	76.7±0.1
$E2,M1,E1,M2$	35.5	1.8	1.2±1.3	13.6±0.7	3.7±0.7	81.4±0.4
$E2,E1,M2$	39.9	1.8		11.1±0.2	2.8±1.2	86.1±0.2

[a]Refer to text.

The model predicts the tensor observable $A_{yy}(E)$ at $\theta_{\text{lab}} = 130°$ in Fig. 8 quite well. Whereas at energies higher than about $E_d = 10$ MeV A_{yy} arises from the products of the dominant $^1d_2$ $S=0$ ($E2$) amplitude with the smaller $S=2$ ($E2$) amplitudes, at lower energies the MCRGM model indicates that A_{yy} arises from the interference of two $S=1$ terms (e.g., $E1/E1$ interference).[10]

$A_{yy}(\theta)$ is related to the spherical tensor analyzing powers $T_{20}(\theta)$ and $T_{22}(\theta)$ by the expression given in Eq. (4). Unlike $A_{yy}(\theta)$, which contains the amplitude $^5s_2$ ($A_{s\to S} + A_{s\to D}$) only to second order (the $^5s_2$ amplitude squared), all the $T_{2q}(\theta)$ contain this amplitude in first order. This amplitude ($^5s_2$) is expected to be strongly effected by the deuteron's D state, which is not included in the present MCRGM model calculation. Compared to $A_{yy}(\theta)$, $T_{20}(\theta)$ is sensitive to this amplitude via interference terms over an energy range where the amplitude itself is not large. The current $T_{20}(E,\theta)$ data exist only above $E_d = 5$ MeV and, as seen in Fig. 8, may indicate a broad 2^+ resonance in the vicinity of $E_d = 8$ MeV, although further study (better counting statistics) in this energy region is required before a conclusion can be reached. Above 8 MeV the MCRGM calculation describes the trend of the data for both $A_{yy}(E)$ and $T_{20}(E)$ quite well.

$T_{20}(\theta)$ at 14.7 MeV is shown in Fig. 9. The MCRGM calculation does a good job of describing $T_{20}(\theta)$ as a function of angle at both 10 MeV (Ref. 9) and 14.7 MeV. Polarization observables appear to be the most sensitive means for distinguishing between the amplitudes at low energies. Future experiments may include measuring $T_{20}(E,\theta)$ and $T_{21}(E,\theta)$ and other observables at low energies, with the goal of improving energy resolution and counting statistics. Future MCRGM calculations that include the deuteron, ^{3}He, and ^{3}H D states are needed for a proper comparison of theory and experiment.

IV. TRANSITION-MATRIX ANALYSIS

The expressions for the angular distribution of γ rays from capture reactions have been published in detail by Seyler and Weller.[26] The coefficients of the associated Legendre polynomial expansions of the products of the unpolarized cross section with the analyzing powers can be written in terms of the amplitudes and phases of the contributing transition-matrix elements. Using these expressions, all of the available angular distribution data $[\sigma(\theta), A_{yy}(\theta), A_y(\theta), T_{20}(\theta)]$ were fitted simultaneously at each energy in order to extract the amplitudes and phases of the relevant transition-matrix elements.

The transition-matrix element amplitudes and phases (free parameters) we considered essential to the analysis are ($^{2S+1}L_J$ notation)

$$^1d_2\ (E2)+\text{phase angle},\quad ^5s_2\ (E2)+\text{phase angle},$$

$$^5d_2\ (E2)+\text{phase angle},\quad ^5d_1\ (M1)+\text{phase angle},$$

$$^3p_1\ (E1)+\text{phase angle},\quad ^3p_2\ (M2)+\text{phase angle}.$$

TABLE III. Results of fitting the available data simultaneously with selected multipoles at $\langle E_d \rangle = 1.2$ MeV.

Allowed multipole	χ^2	χ^2/ν	Partial contributions to the total cross section (%) by γ multipolarity $E1$	$M2$	$E2$
$E2$	169.9	10.0			100
$E2,E1$	21.2	1.4	40.7±0.1		59.3±1.2
$E2,M2$	35.8	2.4		62.6±0.1	37.4±1.9
No ^{4}He D state[a]	39.8	3.1	0.5±1.2	47.2±0.1	52.3±0.5
$E2,M2,E1$	17.6	1.4	1.8±0.9	50.4±0.1	47.9±1.2

[a]Refer to text.

TABLE IV. Results of fitting the available data simultaneously with selected multipoles, $\langle E_d \rangle \leq 0.8$ MeV.

Allowed multipole	χ^2	χ^2/ν	Partial contributions to the total cross section (%) by γ multipolarity $E1$	$M2$	$E2$
$E2$	41.1	5.2			100
$E2,E1$	11.9	1.9	5.3±2.0		94.7±1.4
$E2,M2$	8.6	1.4		5.1±3.2	94.9±2.7
No ^{4}He D state[a]	15.4	2.5	15.4±1.5	18.4±1.0	66.2±0.9
$E2,M2,E1$	7.0	1.6	16.1±1.3	22.5±1.1	61.4±1.8

[a]Refer to text.

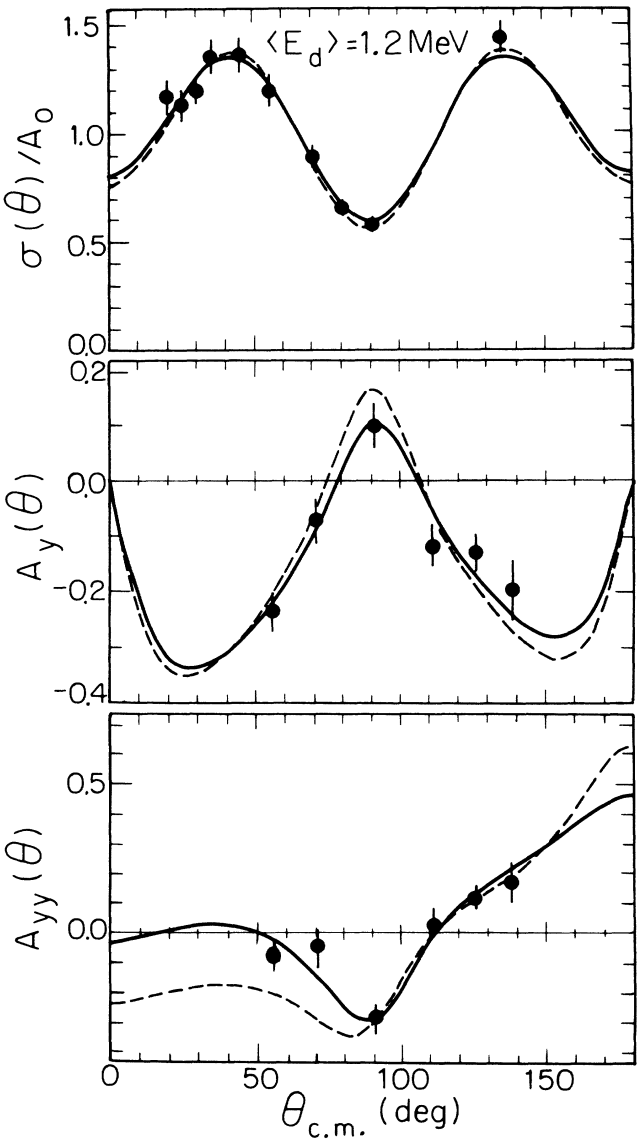

FIG. 10. Angular distributions of the data in the center-of-mass frame for the ^{2}H($\vec{d},\gamma$)^{4}He reaction at $\langle E_d \rangle = 1.2$ MeV. The solid curves denote the full fit (with $E2$, $E1$, and $M2$ multipolarities) whereas the dashed curves are the "no D-state case" [excluding the $^5d_2 \rightarrow {}^5D_0$ ($E2$) transition]. $M1$ transitions have not been included in this figure as the analysis shows they were vanishingly small at this energy. Errors represent the statistical uncertainties associated with the data points.

The phase angle of $^1d_2$ was arbitrarily set to zero because only the difference in phase angles enter the equations.

We present the results of the fitting procedure with selected multipolarities in Tables II–IV. While every combination of multipolarities was examined for its final value of χ^2, only a few are listed in these tables. For example, based on χ^2/ν results (ν is the number of degrees of freedom), we find that pure $E2$ is not a good assumption (e.g., $\chi^2/\nu = 10.0$ at $\langle E_d \rangle = 1.2$ MeV). We report that at least two multipolarities, $E2/E1$ or $E2/M2$, are necessary to give a reasonable value for χ^2/ν. The addition of $M1$ to these combinations is not a clear advantage to these fits; it contributes very little strength. Also it appears that the transition $^5d_2$ ($E2$) is necessary to account for the data at all energies studied here. Assuming that the $^5d_2$ ($E2$) is a $\Delta S = 0$ transition and neglecting tensor force effects in the continuum, this transition should populate the $^5D_0$ state of ^{4}He exclusively. To illustrate this, the rows of Tables II–IV labeled "no D state" included all the partial waves except $^5d_1$ ($M1$) and $^5d_2$ ($E2$)$\rightarrow {}^5D_0$. An example of the simultaneous fits to the angular distribution data at $\langle E_d \rangle = 1.2$ MeV is shown in Fig. 10; the solid curve is the fit with $E2$, $E1$, and $M2$ multipolarities and the dashed curve is the "no ^{4}He D state" case.

At 14.7 MeV (Table II) the main difference between the model and the fits is the strength of the $E2$ transitions. The fits favor solutions with less $E2$ strength and more $E1$ ($\sim$13%) strength, whereas the model places over 95% of the total strength in the $E2$ transitions. The fits with $E2$, $M1$, $E1$ multipoles or $E2$, $M1$, $M2$ look similar to the model in the distribution of strengths. However, measurements of $T_{21}(\theta)$ and higher precision data for the other observables may be necessary to clarify this point.

At $E_d = 1.2$ MeV (Table III) there is a very strong indication for the presence of non-$E2$ radiation. The result in Table III using only $E2$ and $E1$ multipoles gives 41% $E1$ and 59% $E2$ strength with a value for χ^2/ν of 1.4. The fit using $E2$, $M2$, and $E1$ multipoles also gives χ^2/ν of 1.4 but attributes 50% to $M2$ strength and only 2% to $E1$ strength. The MCRGM calculation divides the odd multipole strength equally between $E1$ and $M2$ and gives a total odd multipole strength of around 40%. The authors of the MCRGM calculation[4] state that the only transition which reflects solely the D state in ^{4}He is $M1$, as these channels do not decay to the S-state component. We find from the transition-matrix analysis that the $M1$

transition $^5d_1$ $(M1)\rightarrow{}^5D_0$ appears to be vanishingly small at low energies.

At less than 0.8 MeV, the fit produces values for strengths that are nearly equally divided between each of the partial waves considered, between 15% and 25% each. The most surprising feature of this result is the large value for the $^5d_1$ $(E2)$ transition (21%), which is greater than the $^1d_2$ $(E2)$ transition (16%). The MCRGM model calculation does not show this result. The *ratio* of the amplitudes $E1$ to $M2$ is very nearly equal for the MCRGM calculation and the fit, but the odd multipole strength is much larger in the model.

V. CONCLUSIONS

We have measured the $^2\mathrm{H}(\vec{d},\gamma)^4\mathrm{He}$ reaction observables $\sigma(\theta)$, $A_y(\theta)$, $A_{yy}(\theta)$, and $T_{20}(\theta)$ over several energies below $\langle E_d(\mathrm{lab})\rangle = 15$ MeV. Measurements of the absolute cross section were made in many cases with an uncertainty of $\pm 15\%$. Statistical uncertainties dominate the errors involved in measurements of the polarization observables. At bombarding energies near 10 and 15 MeV, the reaction is dominated by d-wave capture to the $^1S_0$ state of ^{4}He while s- and d-wave $E2$ capture to the $^5D_0$ state of ^{4}He is the most important factor determining the large tensor analyzing powers.

The MCRGM calculation can successfully account for much of the present data, especially $A_{yy}(\theta)$ and $T_{20}(\theta)$. The failure of the MCRGM model in reproducing the back-angle behavior of A_y is probably due to the fact that the calculated d-d threshold is too low in energy, which results in an $E1$ and/or $M2$ strength that is too large.[10] The MCRGM calculation will benefit from a more realistic nucleon-nucleon force and the inclusion of D states in all of the fragments. In the MCRGM calculation, only the $^5d_1$ $(M1)\rightarrow{}^5D_0$ transition is directly correlated to the percentage D state in ^{4}He. We find from the transition-matrix analysis that the contribution of $M1$ strength is small ($\sim 1\%$) at 15 MeV and decreases with lower energies.

The result of the MCRGM model calculation for the D state arising from the relative motion between two deuterons in ^{4}He is $P_D = 2.2\%$. To compare this result to other model-dependent estimates of P_D requires that the $(d+d)$ projection of the ^{4}He wave function be analyzed for $L=2$ strength. The theoretical calculations of Ballot[27] and Goldhammer[28] are 13% and 5.4%, respectively, for the ^{4}He nucleus, but these values are for the full D-state probability in ^{4}He and therefore are only upper limits for the present results. The recent results of Carlson[29] with the Green's-function Monte Carlo method for $A=4$ indicate a D-state probability in ^{4}He ranging from 12 to 17.5% with the variation arising from the choice of the N-N interaction. The two-deuteron component must be projected out of these wave functions before a comparison with the present results can be made.

Finally, the experience with this reaction leads us to believe that other capture reactions deserve to be studied more fully at low energy to assess the effects of tensor forces and their role in nuclei and reaction phenomenology and astrophysics. For example, it has been stated that because the value of $S(0)$ for the $^2\mathrm{H}(d,\gamma)^4\mathrm{He}$ reaction is over 30 times higher than previously estimated, inhomogeneous models of big-bang nucleosynthesis may be altered.[4] A more likely result is the net *production* of deuterium from the $^4\mathrm{He}(\gamma,2d)$ process which may occur near active galactic nuclei. The reaction would then have relevance to galactic chemical evolution.[33]

ACKNOWLEDGMENTS

The authors would like to thank Z.D. Huang, J. Feldman, V. Wijekumar, J.C. Riley, R.M. Whitton, J.Z. Williams, M. Balbes, L. Kramer, P. Colby, and E. Hayward for their invaluable assistance in collecting these data and T. Morello, Jr. for assistance in the analysis. H. Hofmann allowed us to have access to the results of the MCRGM calculations. Useful conversations with J.A. Tostevin, D. R. Lehman, G. Hale, N. Jarmie. R. N. Boyd, and A. Arriaga are greatly appreciated. Details of the T-matrix analysis, data acquisition, and direct capture analysis are available elsewhere.[34] The data reported in this paper, including coefficients determined from a Legendre polynomial fit to the data, have been deposited with the Physics Auxiliary Publication Service of the AIP.[35] This work was supported by the U.S. Department of Energy, Office of High Energy and Nuclear Physics, under Contract Nos. DE-AC05-76ER01067 and DE-FG05-88ER40441.

[1]H. R. Weller, P. Colby, N. R. Roberson, and D. R. Tilley, Phys. Rev. Lett. **53**, 1325 (1984).

[2]A. Arriaga, A. M. Eiró, F. D. Santos, and J. E. Ribeiro, Phys. Rev. C **37**, 2312 (1988); A. Arriaga, private communication.

[3]J. A. Tostevin, Phys. Rev. C **34**, 1497 (1986); private communication.

[4]G. Blüge, H. J. Assenbaum, and K. Langanke, Phys. Rev. C **36**, 21 (1987).

[5]J. Piekarewicz and S. E. Koonin, Phys. Rev. C **36**, 875 (1987).

[6]H. R. Weller and D. R. Lehman, Annu. Rev. Nucl. Part. Sci. **38**, 563 (1988).

[7]E. K. Warburton and J. Weneser, in *Isospin in Nuclear Physics*, edited by D. H. Wilkinson (North-Holland, Amsterdam, 1969), p. 175.

[8]D. R. Lehman, R. M. Whitton, and H. R. Weller discuss $E1$ radiation effects due to charge polarization between identical particles, and present a correction to the argument given in Ref. 1 concerning the isospin selection rule for $E1$ transitions (unpublished).

[9]B. Wachter, T. Mertelmeier, and H. M. Hofmann, Phys. Lett. B **200**, 246 (1988), and references therein.

[10]J. L. Langenbrunner, G. Feldman, H. R. Weller, D. R. Tilley, B. Wachter, T. Mertelmeier, and H. M. Hofmann, Phys. Rev. C **38**, 565 (1988); H. M. Hofmann, private communication.

[11]D. M. Brink and G. R. Satchler, *Angular Momentum* (Oxford University Press, Oxford, 1968).

[12]S. Mellema, T. R. Wang, and W. Haeberli, Phys. Lett. **B166**, 282 (1986); Phys. Rev. C **34**, 2043 (1986); Bull. Am. Phys. Soc.

32, 1547 (1987).

[13]L. E. Porter, L. C. McIntyre, and W. Haeberli, Nucl. Instrum. Methods **89**, 237 (1970); see, also, J. C. Duder, J. F. Clare, and H. Naylor, *ibid.* **123**, 89 (1975), which agrees with the present results after normalizing upward by 6%; computer codes for energy loss were based on the equations of H. A. Bethe and J. Ashkin, in *Experimental Nuclear Physics,* edited by E. Segrè (Addison-Wesley, Reading, MA, 1962), Vol. I.

[14]T. B. Clegg, G. A. Bissinger, and T. A. Trainor, Nucl. Instrum. Methods **120**, 445 (1974).

[15]T. A. Trainor, T. B. Clegg, and P. W. Lisowski, Nucl. Phys. **A220**, 533 (1974).

[16]G. Clausnitzer, R. Fleischmann, and H. Wilsch, Phys. Lett. **B25**, 466 (1967).

[17]H. Cords, G. U. Din, M. Ivanovich, and B. A. Robson, Nucl. Phys. **A113**, 608 (1968).

[18]H. R. Weller and N. R. Roberson, IEEE Trans. Nucl. Sci. **NS-28**, 1268 (1981).

[19]W. Haeberli, in *Nuclear Spectroscopy and Reactions,* edited by J. Cerny (Academic, New York, 1975), Pt. A, p. 15.

[20]G. G. Ohlsen, P. A. Lovoi, R. A. Hardekopf, R. L. Walter, and P. W. Lisowski, Nucl. Instrum. Methods **131**, 489 (1975).

[21]H. A. Grunder, R. Gleyvod, J. Lietz, G. Morgan, H. Rudin, F. Seiler, and A. Stricker, in *Polarization Phenomena in Nuclear Reactions,* edited by H. H. Barschall and W. Haeberli (The University of Wisconsin Press, Madison, 1970), p. 506; for values of a tensor analyzing power for the $T(d,n)^4$He reaction with polarized deuteron energy below 100 keV, see G. G. Ohlsen, J. L. McKibben, and G. P. Lawrence, *ibid.*, p. 503.

[22]H. R. Weller, P. Colby, J. Langenbrunner, Z. D. Huang, D. R. Tilley, F. D. Santos, A. Arriaga, and A. M. Eiró, Phys. Rev. C **34**, 32 (1986).

[23]W. E. Meyerhof, W. Feldman, S. Gilbert, and W. O'Connell, Nucl. Phys. **A131**, 489 (1969).

[24]R. W. Zurmühle, W. E. Stephens, and H. H. Staub, Phys. Rev. **132**, 751 (1963).

[25]A. J. Ferguson, *Angular Correlation Methods in Gamma-Ray Spectroscopy* (North-Holland, Amsterdam, 1965).

[26]R. G. Seyler and H. R. Weller, Phys. Rev. C **20**, 453 (1979).

[27]J. L. Ballot, Phys. Lett. **127B**, 399 (1983).

[28]P. Goldhammer, Phys. Rev. C **29**, 1444 (1984).

[29]J. Carlson, Phys. Rev. C **38**, 1879 (1988).

[30]C. A. Barnes, K. H. Chang, T. R. Donoghue, C. Rolfs, and J. Kammeraad, Phys. Lett. B **197**, 315 (1987).

[31]F. J. Wilkinson III and F. E. Cecil, Phys. Rev. C **31**, 2036 (1985).

[32]A. Degré, M.Sc. thesis, Université de Strasbourg, 1969.

[33]R. N. Boyd, G. J. Ferland, and D. N. Schramm, Astrophys. J. **336**, L1 (1989).

[34]J. L. Langenbrunner, Ph.D. dissertation, Duke University, *Radiative Capture of Polarized Deuterons by Deuterium Below 15 MeV* (University Microfilms International, Ann Arbor, Michigan, 1989).

[35]See AIP document PAPS PRVCA-42-1214-6 for six pages of the tabulated data; they include and supercede the data of Ref. 22 (PAPS PRVCA-34-32-2). Order by PAPS number and journal reference from American Institute of Physics, Physics Auxiliary Publication Service, 335 East 45th Street, New York NY 10017. The price is $1.50 for each microfiche (98 pages) or $5.00 for photocopies of up to 30 pages, and $0.15 for each additional page over 30 pages. Airmail additional. Make checks payable to the American Institute of Physics.

[36]H. R. Weller, R. M. Whitton, J. L. Langenbrunner, E. Hayward, W. R. Dodge, S. Kuhn, and D. R. Tilley, Phys. Lett. B **213**, 413 (1988).